Chemical Engineering Journal 165 (2010) 934–945

Contents lists available at ScienceDirect

Chemical Engineering Journal

journal homepage: www.elsevier.com/locate/cej

Design of automotive flow-through catalysts with optimized soot trapping capability

Henrik Ström[a,b,*], Srdjan Sasic[c], Bengt Andersson[a,b]

[a] Chemical Reaction Engineering, Chalmers University of Technology, SE-412 96 Göteborg, Sweden
[b] Competence Centre for Catalysis, Chalmers University of Technology, SE-412 96 Göteborg, Sweden
[c] Applied Mechanics, Chalmers University of Technology, SE-412 96 Göteborg, Sweden

ARTICLE INFO

Article history:
Received 25 August 2010
Received in revised form 11 October 2010
Accepted 12 October 2010

Keywords:
Diesel soot
Gasoline soot
Particulate matter
Automotive catalyst
Monolith
Computational fluid dynamics (CFD)

ABSTRACT

A hybrid model for accurate and computationally efficient simulations of the particle trapping characteristics of automotive flow-through catalysts is suggested in this paper. The new model is validated against the performance of a more elaborate, but computationally far more expensive model.

In this hybrid model, the trapping of the smallest particles is predicted using a computationally efficient submodel that can also be used for screening of new catalyst substrate designs. It is shown here that this screening model is very accurate for particles smaller than approximately 50 nm. A number of different catalyst designs are evaluated and compared using the screening model. In particular, the performance of a promising channel design with porous obstacles is evaluated. This design could potentially give over 70% reduction of small soot particles without a substantial increase in the pressure drop.

1. Introduction

Particulate matter is formed during incomplete combustion in modern diesel and gasoline engines. When emitted to the ambient air, these submicron-sized particulates may end up in human lungs. It is estimated that one hundred thousand people die prematurely every year in Europe alone due to particulate matter from human activities [1]. In order to improve the air quality, forthcoming emission legislation for vehicles will focus not only on regulating the total mass of particulate matter emitted, but also the number of particles [2]. It is therefore likely that there will be a need to optimize the automotive emission control systems with respect both to the number and the mass of the particles emitted.

The so-called wall flow particulate filters in use today are very efficient, but still have unresolved issues regarding robustness and regeneration strategy. They also impose a fuel penalty by a marked increase in the total pressure drop over the exhaust gas aftertreatment system. It has been reported that particles smaller than 110 nm may be able to pass through the wall-flow filter uncollected [3]. A recent experimental study revealed a minimum in the particle trapping efficiency for particles of size around 100 nm in both cordierite and SiC wall-flow filters [4]. The possibility to introduce specific, application-tailored particle trapping capabilities to a preceding flow-through filter (e.g. the diesel oxidation catalyst or the three-way catalyst in gasoline applications) is therefore very attractive.

The different types of particulate matter have been shown to behave very differently in the exhaust catalyst [5]. Therefore, in order to optimize the overall trapping of particulate matter, a number of different measures will have to be undertaken. The purpose of the current work is twofold: (a) to identify these measures and (b) to find an optimal design tool for automotive oxidation catalysts depending on which type(s) of particulate matter one wishes to target specifically.

2. Background

In this paper, we will first motivate the introduction of particle trapping capabilities to the oxidation catalyst from the perspective of the overall performance of the aftertreatment system. We then use the previously published detailed model of Ström and Andersson [5] to evaluate the relative influence of the phenomena taken into account in that model. The results from this evaluation is used to suggest a new, simpler model. The performance of the simpler model is then compared to that of the full model, and a hybrid model is proposed that takes advantage of both the computational efficiency of the simpler model and the detailed information from the full model. A broad scanning of six geometrical designs of the

* Corresponding author at: Chemical Reaction Engineering, Chalmers University of Technology, SE-412 96 Göteborg, Sweden. Tel.: +46 317722982.
E-mail addresses: henrik.strom@chalmers.se (H. Ström), bengt.andersson@chalmers.se (B. Andersson).

1385-8947/$ – see front matter © 2010 Elsevier B.V. All rights reserved.
doi:10.1016/j.cej.2010.10.026

Nomenclature

C_c	Cunningham correction factor
D	diffusivity ($m^2\ s^{-1}$)
D_p	pore diameter (m)
d_c	unit collector diameter (m)
d_h	hydraulic diameter (m)
d_p	particle diameter (m)
E	number trapping efficiency
g	gravitational acceleration ($m\ s^{-2}$)
$g(\varepsilon)$	geometric function
k_B	Boltzmann constant ($J\ K^{-1}$)
L	length (m)
m_p	particle mass (kg)
N_R	interception parameter
n	number of particles
P	pressure (Pa)
Pe	Peclet number
r	radial position (m)
Sh	Sherwood number
St	Stokes number
T	temperature (K)
t	time (s)
U	mean velocity ($m\ s^{-1}$)
u	velocity ($m\ s^{-1}$)
x	position (m)
x_i	mass fraction of species i
ε	porosity
η_{DR}	trapping efficiency due to Brownian motion and inertial effects
η_D	trapping efficiency due to Brownian motion
η_R	trapping efficiency due to inertial effects
μ	viscosity (Pa s)
ρ	density ($kg\ m^{-3}$)
ρ_p	particle density ($kg\ m^{-3}$)
τ_p	particle relaxation time (s)
τ_s	characteristic time scale (s)
Ω	rotational velocity (s^{-1})

oxidation catalyst is then carried out using the simpler model. These designs are motivated by a preceding theoretical analysis, and include both designs previously discussed in the literature as well as novel ones suggested here. The designs are compared in a results map, from which the most fuel efficient designs can be discerned. The possibility to further optimize these designs is finally discussed.

3. Advantages of particle trapping in the oxidation catalyst

We aim here to propose a strategy for the design of traditional automotive catalysts aiming to keep high the overall particle trapping efficiency of the complete exhaust gas aftertreatment system while keeping the fuel penalty to a minimum. In addition, the full system should be robust and reliable. It therefore becomes necessary to investigate what measures that can be undertaken in the oxidation catalyst to lower the pressure drop over a succeeding particulate filter and to increase its performance predictability.

When a conventional wall-flow particulate filter is clean (i.e. before the soot cake is formed), the most significant contribution to the pressure drop is caused by the gas flowing through the porous walls. The pressure drop over the wall can be estimated from Darcy's law with a Kozeny–Carman correlation for the permeability of the filter material, where D_p is the wall pore diameter and ε the effective porosity [6]:

$$\frac{\Delta P}{L} = 5.6\frac{\mu U}{\varepsilon^{5.5} D_p^2} \tag{3.1}$$

When the filter is loaded with soot, it is the soot content on and inside the channel walls that causes most of the pressure drop. The well-known Ergun equation gives the pressure drop for the flow through a porous bed (e.g. soot deposition layer) constituted of spherical particles of uniform size d_p:

$$\frac{\Delta P}{L} = 150\frac{(1-\varepsilon)^2 \mu U}{\varepsilon^3 d_p^2} + 1.75\frac{(1-\varepsilon)\rho U^2}{\varepsilon^3 d_p} \tag{3.2}$$

It should be stressed here that Eq. (3.2) is only an approximation of the pressure drop in the real application. In reality, a range of complex phenomena (e.g. degree of soot cake compaction, possible soot migration and blow-off effects) may influence the actual pressure drop. Eq. (3.2) is thus only used here as the basis for a qualitative discussion.

It is then evident from Eqs. (3.1) and (3.2) that a more densely packed soot bed and/or a more densely filled porous wall will cause significantly higher pressure drops. The effective porosities will be very much influenced by the smallest particles, as they will fill the voids in between the larger particles and inside the smallest pores. A reduction of the number of very small particles passed on from the oxidation catalyst to the particulate filter therefore has a large potential to decrease the pressure drop over the filter.

In addition, removal of the largest particles will significantly reduce the rate of soot accumulation in the filter, which will decrease the regeneration frequency. If the accumulation of soot is low enough, active regeneration of the filter may even be omitted.

Even in a situation where the new design of the oxidation catalyst channels causes an increase in pressure drop that outweighs the pressure drop gain in the wall-flow filter, the particle content of the filter will have a more narrow size distribution. For diesel and gasoline particulate matter, the particles of different size typically differ also chemically [7]. Since the oxidation behavior is largely dependent on the type of particles present, a more narrow compositional distribution will enhance the robustness and predictability of operation for the filter.

In addition, for gasoline applications it might be sufficient to remove a large fraction of the smallest particles to comply with emission regulations, as gasoline exhaust generally contains fewer and smaller particles than diesel exhaust [7]. A properly designed three-way catalyst may then spare the addition of a particulate filter altogether.

4. Solving for the gas flow

The work presented herein is based on modeling and simulation using computational fluid dynamics (CFD). Since the Reynolds numbers typically encountered in the flow of exhaust gases through monoliths are of the order of a couple of hundreds, it is possible to use a laminar flow model and solve the continuity equation with the incompressible Navier–Stokes equations:

$$\nabla \cdot u = 0 \tag{4.1}$$

$$\rho\left[\frac{\partial u}{\partial t} + \nabla\cdot(uu)\right] = -\nabla P + \nabla\cdot\left[\mu\left(\nabla u + \nabla u^T\right)\right] + \rho g \tag{4.2}$$

The boundary conditions used are that of a constant velocity over the inlet, a constant (atmospheric) pressure over the outlet, and no-slip at all walls. A constant velocity over the inlet is deemed a realistic inlet boundary condition since the dimensions of the channels are small in relation to the velocity gradients of the mean flow upstream the catalyst. In addition, the transition to a fully

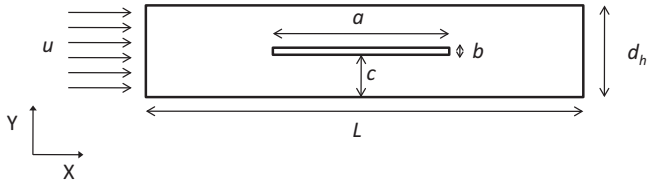

Fig. 1. Illustration of the test geometry. The values used are: $u = 10\,\mathrm{m\,s^{-1}}$, $L = 5$ mm, $d_h = 1$ mm, $a = 2$ mm, $b = 0.1$ mm and $c = 0.45$ mm.

developed laminar flow profile occurs over a very short distance (of the order of millimeters) at the prevailing Reynolds numbers (cf. [8]). The particles are treated differently depending on the model used, as discussed in the subsequent sections.

5. Analysis of the particle transport phenomena using a detailed model

In the elaborate model of Ström and Andersson [5], the different particle transport mechanisms are taken into account via the modeling of five different forces. These are: the drag force, the lift force, the van der Waals-interaction force, the buoyancy force and the Brownian motion. In order to assess the relative importance of these forces, their respective contribution to the overall particle trapping efficiency is examined for a generic geometry. This geometry is a two-dimensional channel (i.e. flow between parallel plates) into which a third plate of finite thickness is positioned. The geometry is illustrated in Fig. 1. Note that this geometry does not represent an entire monolith channel (but rather a few percent of one) and that the reported trapping efficiencies therefore are only relative measures to compare the different trapping mechanisms. The inner plate is included to constitute an obstacle. The domain only has to be sufficiently long for us to be able to get an estimate of the influence of the different mechanisms on the particle trapping efficiency. This geometry is referred to as the 'test geometry'.

In each simulation, 110 000 particles (from 5 nm to 10 μm) are released evenly over the inlet. This means that inlet effects are neglected altogether. Although interesting, the fluid dynamic phenomena involved in creating the inlet effects are too complex to be investigated within the current work. These phenomena include the drastic decrease in the characteristic length scale bounding the flow, leading in turn to a transition from turbulent to laminar flow, and an acceleration of the gas due to the decreased area available for fluid flow (an effect stemming from the presence of the monolith walls).

All particles are assumed to have a density of $1000\,\mathrm{kg\,m^{-3}}$. Gravity is assumed to act in the negative Y-direction (cf. Fig. 1). As shown by Ström and Andersson [5], the variation of the particle trapping efficiency with temperature and gas velocity is relatively small. It is therefore sufficient to study a single representative temperature (300 °C) and velocity ($10\,\mathrm{m\,s^{-1}}$). The flow field is assumed stationary and is kept frozen as the particles are tracked through it. The presence of the particles is assumed not to have any effect on the gas.

The particle number trapping efficiency, E, is evaluated as:

$$E = \frac{n_{trapped}}{n_{total}}, \tag{5.1}$$

where $n_{trapped}$ is the number of particles trapped at the wall in the simulation and n_{total} is the total number of tracked particles. The results for the test geometry is shown in Fig. 2. Since the model for the Brownian motion includes random numbers, care must be taken in order to ensure that the simulation results are independent of the number of particles used and the seed to the random number generator. The results presented in Fig. 2 show the mean from three simulations with three different randomization seeds, with the error bars indicating a 95% confidence interval.

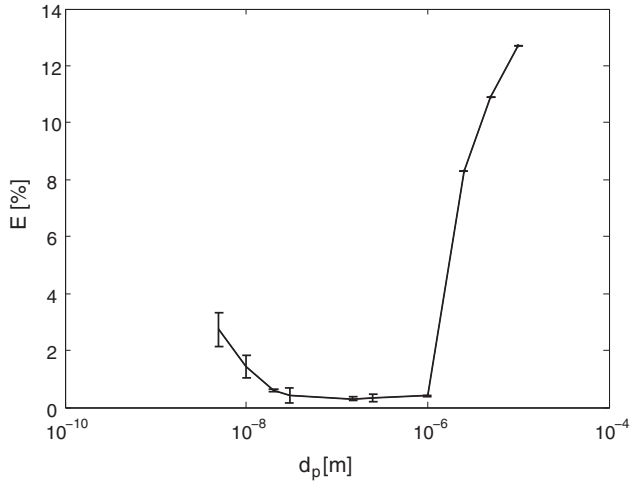

Fig. 2. The particle trapping efficiency in the test geometry according to the full model of Ström and Andersson [5]. The error bars indicate the 95% confidence interval for the results after three successive simulations with different seeds to the random number generator.

When the particles have a long enough response time, they will not be able to follow the fluid flow past an obstacle, such as the inner plate in the test domain. They are therefore trapped on the edges of the plate. It is also evident that for the larger particles, there is a quite narrow interval when the particle response time becomes long enough for particles to be trapped on the plate (there is a 'kink' in the particle trapping efficiency curve between 1 μm and 2.5 μm). The Brownian motion works in another way, so that the trapping of smaller particles increases exponentially with decreasing particle diameter. There is thus no such clear onset of when the Brownian motion becomes the dominating trapping mechanism. It can also be seen that there is no change in the predictions of the trapping efficiency of particles larger than one micrometer when the random number generator seed is varied, indicating that the Brownian motion is insignificant for these particles.

If the particles were massless tracers, they would simply follow the fluid streamlines through the domain and the trapping efficiency would be zero. That is, every contribution to the total trapping efficiency must come from the effect of the different forces acting on the particles. It is also possible that two or more forces interact so as to create some synergic effect. Therefore, it is more relevant to study the effect of each force as it is removed from the Lagrangian force balance rather than to study the effect of isolated forces. The particle trapping efficiency due to a certain force on the particles, E_{F_i}, can then be calculated as:

$$E_{F_i} = E_{with} - E_{withouth}, \tag{5.2}$$

where E_{with} and $E_{without}$ are the total particle trapping efficiencies with and without the force F_i, respectively. Note that it is also perfectly possible for E_{F_i} to become negative (which should be interpreted as that the force in question is counteracting deposition).

Since we want the particles to have information about the flow field, the drag force is always included and its individual effect is not monitored. This is not a problem since the drag force is computationally cheap and its formulation in the Lagrangian force balance stands on solid theoretical ground.

It should be noted here that whereas all other forces in the model of Ström and Andersson [5] contain no particle material properties other than the density, the value of the Hamaker constant in van der Waals interaction is a property of the combined particle-

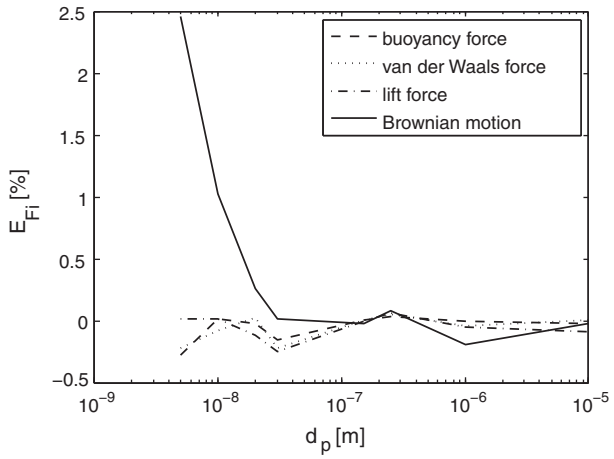

Fig. 3. The particle trapping efficiency due to an indicated force according to the model of Ström and Andersson [5].

gas-surface system and could therefore change depending on the circumstances. However, the order of magnitude of the constant used here is essentially the same for all relevant materials, hence the order of magnitude of the van der Waals force as estimated here is considered reasonable.

The result of the investigation of the effect of the individual forces is shown in Fig. 3. It is once again shown that the Brownian force is the dominating force for the smallest particles (cf. Figs. 2 and 3). The variation in predicted trapping efficiency is small when removing any other force. Since E_{F_i} is small for all forces for large particles, it is evident that the high trapping efficiency for those particles is caused by inertial effects.

The results obtained from this analysis shall now be used in the construction of a more computationally efficient model.

6. A simplified model for screening and optimization

Simulations of particle trapping with the elaborate model are time consuming (up to several days on a desktop computer) which limits the number of designs that can be evaluated in a reasonable time. To be able to efficiently screen a multitude of geometrical designs, it is desirable to find a simpler model that is still accurate enough to provide a good first estimate. Moreover, if one aims not only at screening different designs, but also at optimizing a chosen design idea, then a faster model is absolutely necessary.

To solve for the flow field inside a monolith channel is computationally cheap compared to tracking a large number of individual particles subjected to Brownian motion. A computationally efficient approach would therefore be if one could use a passive scalar to get an estimate of the trapping efficiency. Chandrasekhar [9] discussed an analogy between random flight (i.e. Brownian motion) and diffusion, and showed that the motion of a large number of individual particles subjected to random flights without mutual interference can be described as a diffusion process. The boundary conditions for a surface which is a perfect absorber then becomes that the concentration should be equal to zero. We therefore suggest that the particle trajectories of many small particles of Brownian diffusivity D_i can be estimated by solving the following species transport equation:

$$\frac{\partial x_i}{\partial t} + \mathbf{u} \cdot \nabla x_i = D_i \nabla^2 x_i \tag{6.1}$$

Here, x_i represents the mass fraction of particulate phase i in a computational cell. By introducing several different particulate phases (each with their associated values of D_i), the particle trapping efficiencies of several different particle types can be estimated simultaneously. The Brownian diffusivity is given by [10]:

$$D_i = \frac{k_B T C_c}{3\pi\mu d_p}. \tag{6.2}$$

The transport equation (6.1) is to be solved subject to the following boundary conditions:

$$x_i = x_i^* \quad \text{on the inlet, and} \tag{6.3}$$

$$x_i = 0 \quad \text{on all walls.} \tag{6.4}$$

Here, x_i^* is an arbitrarily chosen mass fraction. Since the species i is a passive scalar, the fluid properties are not affected by the chosen value of x_i^*. In essence, it need only be high enough to ensure the changes in concentration throughout the domain are above machine precision. That the mass fraction of species i is zero at all walls is equivalent to assuming that all particles deposit upon contact with the wall, that the trapping efficiency is not a function of the state of the surface and that no significant layer of particulate matter is build up (cf. [9]).

The particle trapping efficiency, E, is then obtained as

$$E = 1 - \frac{\bar{x}_{i,outlet}}{x_i^*}. \tag{6.5}$$

The performance of the simpler method for the test case is compared to the full elaborate model in Fig. 4. Note the excellent predictions for small particles (i.e. fully within the 95% confidence interval given in Fig. 2). As is clearly seen from Fig. 4, however, the effects of inertia on the behavior of the largest particles cannot be described by the simple model.

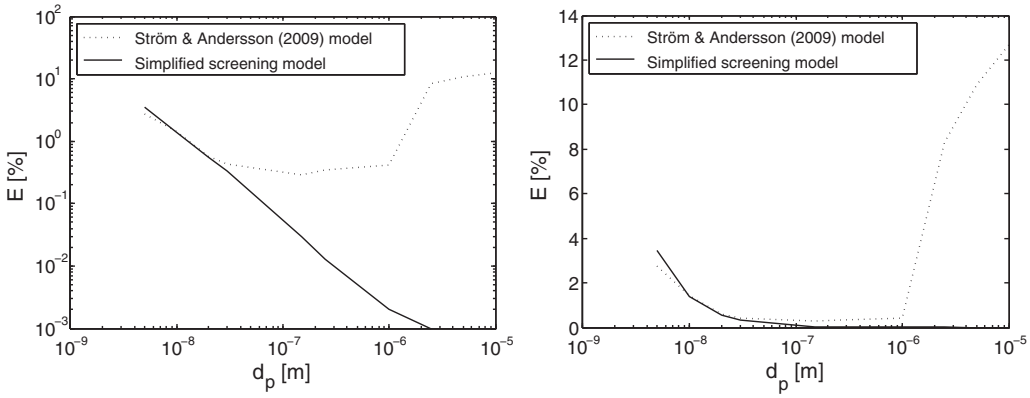

Fig. 4. The particle trapping efficiency (E) for the test case as predicted by the full model of Ström and Andersson [5] and by the simplified screening model proposed here. To the left: in log–log scale. To the right: in semi-log scale.

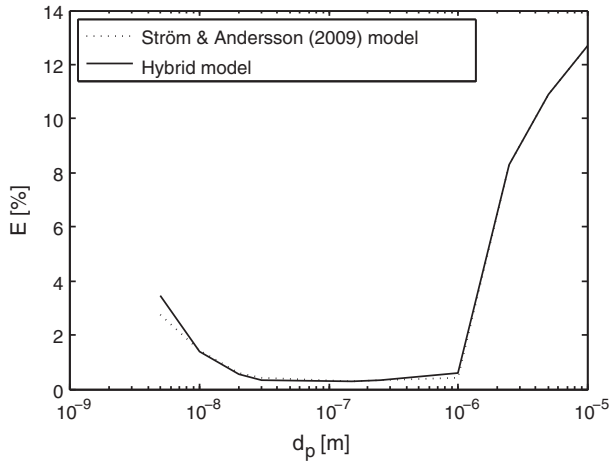

Fig. 5. The particle trapping efficiency (E) for the test case as predicted by the full model of Ström and Andersson [5] and by the hybrid model proposed here.

The method proposed here is superior to the Lagrangian particle tracking approach with regard to computational efficiency, but will fail to describe any effects caused by inertia. Because of the boundary condition used, it is also not possible to obtain the patterns of particle deposition over the substrate or the deposition velocities. The main advantage is thus the fast estimation of the trapping efficiency. In fact, on a desktop computer, the screening model may be two orders of magnitude faster.

7. A hybrid model for efficient and accurate predictions

If the particle trapping efficiency of one type of particle has no influence on the trapping efficiencies of others, and there is no feedback of information from the behavior of individual particles to the flow field (and thus to the pressure drop), it becomes possible to separate the prediction of the particle trapping efficiencies in whichever way one finds appropriate. This separation is what we here refer to as a hybrid model.

We propose that the screening model can be used to estimate the particle trapping efficiency of particles up to 50 nm in diameter (cf. Fig. 4). The detailed model should then be used for particles up to 1 μm. For particles larger than 1 μm, inertial effects are totally dominant, so that drag and gravity are the only forces necessary to consider (cf. Fig. 3). Since the smallest particles are the most computationally demanding to consider with the full model, this hybrid model allows for an excellent balance between accuracy and computational efficiency. The full model is to be used only where the highest sensitivity to the full range of particle motion phenomena is present.

The advantage of the proposed hybrid model is that it captures the inertial effects on the fates of the largest particles, whilst cutting the overall simulation time by at least an order of magnitude (from days to hours). The performance of the hybrid model as suggested here is compared to the results of the full model in Fig. 5.

Since the screening model has been validated in the test geometry, we would also briefly like to assess its validity for more complex geometries. In other words, we want to investigate whether it is possible that any of the phenomena not taken into account in the screening model can become important for particles of diameter smaller than 50 nm. We believe that this is not the case in the present work. Gravitation is known to be an insignificant collection mechanism for small particles [11], and the lift force can be shown to be negligible in magnitude compared to the drag force for particles in the size range of interest [12]. The van der Waals interactions are only acting on very short distances (on the order of the particle size), so that particles in most of the domain are not influenced by the van der Waals-force. Finally, inertial effects become important if there is a time scale of fluid motion comparable to the particle relaxation time. For inertial effects to influence the motion of small particles there thus has to be a fluid time scale on the order of tens of nanoseconds. This is not realistic, but can also be verified a priori from the solution to the gas flow field. In conclusion, we believe that the screening model can safely be used also for more complex catalyst geometries than the test geometry.

8. Design criteria

We have now suggested a hybrid model that can be used to estimate the trapping efficiency of particulate matter over the whole size range encountered in aftertreatment system devices. In other words, we have established our design tool, and now we wish to use this tool to scan a number of proposed catalyst designs. We shall therefore briefly discuss how the standard monolith design may be altered to increase the deposition efficiency.

8.1. Brownian motion

For the smallest particles, Brownian motion is the dominating trapping mechanism [5,11]. The way to increase the trapping of small particulates is thus to secure that each fluid element passing through the catalyst has long enough retention time in close enough proximity to the catalyst wall. An estimate of the displacement due to Brownian motion is provided by:

$$\Delta x = \sqrt{2Dt} \tag{8.1}$$

where D is the Brownian diffusivity [10]. In order for a small particle to have time to deposit, this displacement must at least equal the distance to the closest wall for a time equal to the retention time in the proximity of the wall. The design criterion, if using averaged terms over the entire catalyst, becomes:

$$\frac{2\Delta x}{d_h} = \frac{2}{d_h}\sqrt{2D\frac{L}{U}} \geq 1. \tag{8.2}$$

From this we can conclude that in order to increase particle deposition due to Brownian motion, we can do one or more of the following:

- Decrease the hydraulic channel diameter (d_h).
- Increase the length of the channel (L).
- Decrease the flow rate through the channel (i.e. decrease U).

8.2. Inertial effects

For large particles, inertial effects is the dominating trapping mechanism [5,11]. The most efficient way to trap large particles should thus be to introduce properly designed obstacles to disturb the flow. The tendency for a particle to not be able to avoid an obstacle in the flow is governed by the Stokes number, defined as:

$$St = \frac{\tau_p}{\tau_s} \tag{8.3}$$

where τ_p is the particle relaxation time and τ_s is a characteristic time scale of the flow. It is a good assumption that the particle Reynolds numbers will be small so that the flow around the particle can be approximated by Stokes flow. The particle response time is then given by:

$$\tau_p = \frac{\rho_p d_p^2 C_c}{18\mu}. \tag{8.4}$$

As the characteristic time scale of the flow, the proper choice is the time the gas needs to change direction in front of an obstacle. These time scales can be accurately derived from relatively simple single phase CFD simulations. The design criterion becomes:

$$St = \frac{\rho_p d_p^2 C_c}{18\mu\tau_s} \geq 1. \quad (8.5)$$

From this analysis we see that in order to increase particle deposition due to inertial impaction, we should decrease the system response time at an obstacle. This corresponds to properly designing the obstacle and/or increasing U.

8.3. Radial transport

Medium sized particles are the most difficult particles to trap in a flow-through device [5]. They are too large to effectively diffuse by the Brownian motion to the available surfaces on a time scale comparable to that of the smallest particles, and at the same time they have too little inertia to be readily trapped by inertial effects. Yet, without radically altering the design (such as by introducing electrostatic particle trapping), these are the two main mechanisms with which the medium sized particles must be reached.

Earlier studies on altered channel designs in monolithic reactors have shown the appearance of oppositely rotating vortices after the introduction of obstacles in sinusoidal channel geometries [13]. The influence of such flow patterns on the deposition of particulate matter inside the monolithic channel has however not been studied previously. Particles inside a rotating flow loop will experience a centrifugal force of magnitude $m_p\Omega^2 r$, where Ω is the magnitude of the flow circulation and r is the radial position in the loop. This force will accelerate the particles outwards from the eddy (loop). The distance to the closest wall is then measured from the center of the loop rather than from the center of the channel, i.e. there is a reduction also in the radial distance that the particle needs to migrate. It is clear that the main parameters governing the performance of this type of radial transport will be the magnitude of the flow circulation (Ω) and the lifetime of the flow loop.

9. Geometric designs

9.1. Possible designs

A standard monolith has straight, square channels, whose corners are rounded by the catalyst washcoat. The flow is laminar. The fully dominating mechanism for bringing particles to the channel walls under these circumstances is Brownian diffusion [11]. Based on the reasoning in the previous section, the following changes to the standard design can be proposed:

- Decreasing the hydraulic channel diameter by either reducing the channel diameter (*Design 1*) or introducing new surfaces parallel to the flow inside the channel (*Design 2*).
- Enhancing the radial mixing within the channel: In a normal channel, the retention time is shortest in the middle, where there is a maximum in the volumetric flow rate and the distance to the walls is the longest. By enforcing flow also in the radial direction this situation is changed for the better. This is usually done via the introduction of obstacles, i.e. the utilization of flow loops (*Design 3*). Obstacles may also trap the largest particles because of their inertia.
- Creating secondary flow in the channel by changing the wall surfaces from being perfectly smooth to having e.g. submerged patterns. This approach is similar to that used in plate heat exchangers to enhance heat transfer (cf. *Design 6*).
- Introducing porous parts: If the flow is forced to flow through a porous wall or obstacle, the particle trapping efficiency may be dramatically increased. The porous part need not block the entire flow path, but can be designed as to only partially block the flow (e.g. *Design 4*).
- Irregular channel: Making the channel deviate from the standard straight design may help increase the trapping of larger particles via inertial mechanisms and the trapping of smaller particles due to mixing in the secondary flow (*Design 5*).

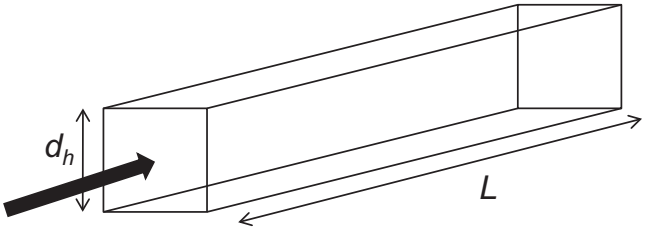

Fig. 6. The layout of Design 1. This design is a standard monolithic channel with square cross-section. The hydraulic diameter (d_h) is equal to the side of the cross-section, and it is varied between 0.2 and 2 mm. The length of the channel (L) is 180 mm. The black arrow indicates the inlet gas flow direction.

We wish to compare the six suggested designs based on their predicted particle trapping efficiency (E) and their pressure drop (ΔP). In order for this comparison to be time-efficient, we use the simplified screening model (Eqs. (6.1)–(6.5)). As this model only takes the Brownian motion into account, it will always predict an exponentially increasing trapping efficiency as the particles become smaller. It is thus sufficient to compare the particle trapping efficiency of a single size of particles to get a comparable figure of merit for each design. Furthermore, we want to demonstrate with great certainty that the screening model is valid and that the reported trapping efficiencies are significantly above machine precision. The conformance with these criteria is enhanced as the particle size decreases. We will therefore investigate the particle trapping efficiency of 5 nm particles, as these constitute the smallest particle size commonly constituting diesel and gasoline particulate matter.

9.2. Reduced channel diameter (Design 1)

Design 1 is illustrated in Fig. 6. Reducing the diameter of a standard monolithic channel will decrease the distance to diffuse, which will increase the trapping efficiency. However, the pressure drop will also increase.

The CFD results for Design 1 will also be compared to theoretical estimations. The trapping efficiency for a diffusing species of diffusivity D in a channel of length L with a scare cross-section of hydraulic diameter d_h may be estimated as:

$$E = 1 - \exp\left(-\frac{4ShDL}{d_h^2 U}\right). \quad (9.1)$$

The Sherwood number, Sh, is calculated from the correlation by Hawthorn [14]. The corresponding pressure drop may be estimated as [15]:

$$\Delta P = \frac{32\mu UL}{d_h^2} + \frac{0.5}{2}\rho U^2. \quad (9.2)$$

9.3. Parallel plates (Design 2)

Design 2 is illustrated in Fig. 7. The idea behind this design is that each fluid element of the gas should pass close to a wall at least at some point during the passage through the channel. This will reduce the distance to diffuse, which will increase the trapping efficiency. Since the plates are not as long as the channel, the pressure drop will be lower than if the overall channel diameter was

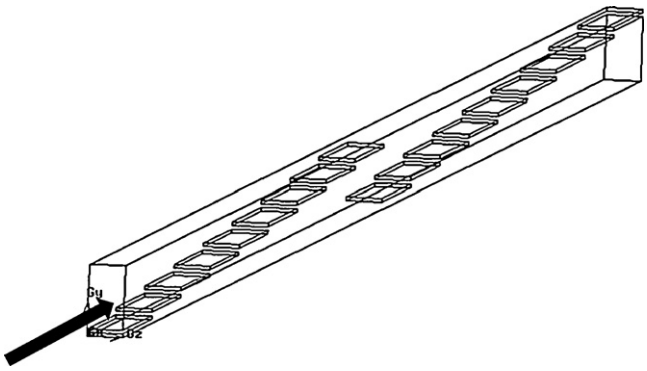

Fig. 7. The layout of Design 2. The exhaust enters through the inlet at the bottom left and flows through the channel and exits at the outlet in the upper right. A symmetry plane cuts the channel in half in the lateral direction (i.e. only half the channel is shown above). The length of the channel is 180 mm and each side in the cross-section is 2 mm. The thickness of a plate is 0.1 mm and also the distance between the plates is 0.1 mm. Each plate is 10 mm long and there are 18 plates in total. The black arrow indicates the inlet gas flow direction.

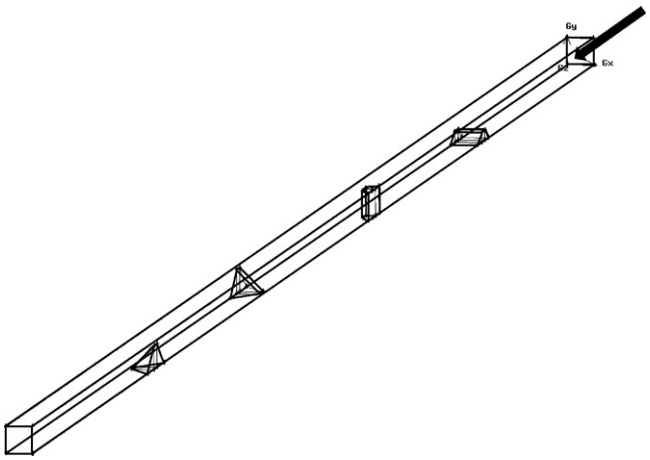

Fig. 9. The layout of Designs 3 and 4. The exhaust enters through the inlet at the upper right and flows through the channel and exits at the outlet in the lower left. The length of the channel is 180 mm and each side in the cross-section is 2 mm. Each obstacle blocks 37.5% of the area perpendicular to the main flow direction and the angle of the slopes up and down the obstacle are 54°. The top of each obstacle is 1 mm long. The black arrow indicates the inlet gas flow direction.

just reduced instead (cf. Design 1). The velocity close to the plates is very low and a short plate length may still be sufficient for the particles to have time to diffuse to the surface.

9.4. Obstacles (Design 3)

The introduction of obstacles into the channel will create flow loops which will enhance the radial mixing. It is very possible that the effect of a flow loop can be either amplified or weakened by the interaction with another flow loop (caused for example by a successive obstacle which is displaced in relation the the obstacle which caused the emergence of the first loop). Building on previous knowledge about flow loops, a scheme for choosing the order and position of obstacles can be established. The following facts are observed (cf. [13]):

- After an obstacle, two flow loops emerge, with a plane of symmetry in between them.
- Each flow loop has a center of rotation, where no fluid displacement will take place.
- In the decision on the location of the next obstacle, it is desirable to place it in such a way that the previous centers of rotation are drawn apart by the newly created flow loops.
- The overall aim is to make sure that no portion of the flow remains at a high velocity without mixing with the rest of the flow for any longer period of time.
- The described problem is to be solved subject to the constraint that the total pressure drop is kept to a minimum.

The suggestion is thus to use a design as illustrated conceptually in Fig. 8. The final layout of Design 3 is depicted in Fig. 9.

9.5. Porous obstacles (Design 4)

The obstacles suggested in Design 3 are solid, so that the gas has to flow over them. Depending on the size of the particles, the time scale for the fluid pathlines rearranging in front of the obstacles may or may not be short enough to cause deposition (cf. Eq. (8.5)). However, if the obstacles themselves are porous, then part of the gas will flow through them. This may enhance particle deposition in two ways, due to both deposition on the front of the obstacle and additional deposition inside the obstacle.

Assuming that the presence of particles inside the obstacle is negligible (i.e. that all particles that enter the obstacle instantly deposit), we can use the screening model to assess the particle trapping efficiency. At the same time, we monitor the total pressure drop over the channel. After we have screened a span of obstacle permeabilities, we shall then evaluate in more detail the most promising one. The permeabilities of a number of porous materials commonly used in exhaust aftertreatment systems are illustrated in Fig. 10 as a reference.

Since we are assuming that all the particles that enter the porous obstacle will be trapped, and since we only simulate trapping and not oxidation, we will have to test that the results obtained under such conditions are realistic. We will do so by using the models for estimating the particle trapping efficiency in a porous material by Konstandopoulos et al. [20] and the model for the particle oxida-

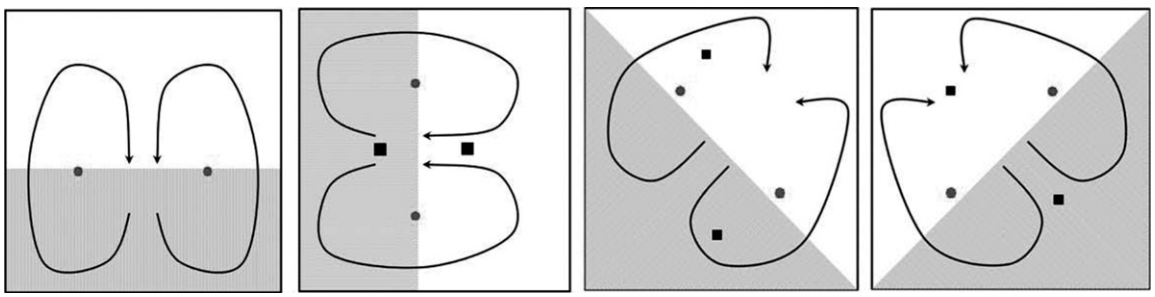

Fig. 8. Flow loops in sequence. The flow pattern is observed from downstream the obstacle (shaded grey). The arrows indicate the fluid motion after the obstacle. Circular dots indicate centers of fluid rotation and square boxes indicate where the previous centers of fluid rotation were positioned.

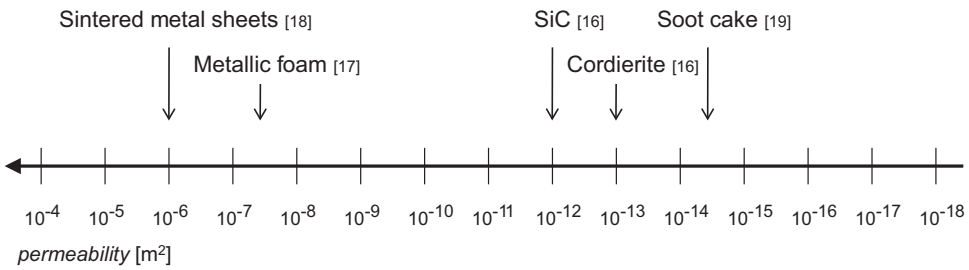

Fig. 10. Illustration of the order of magnitude of permeabilities of common porous materials in exhaust aftertreatment systems. The values for cordierite and SiC are from Cutler and Merkel [16], the value for metallic foam is from Choi et al. [17], the value for sintered metal sheets is from Purem [18] and the value for the soot cake is from Suresh et al. [19].

tion rate suggested by Kandylas and Koltsakis [21]. In this way, we will be able to decide whether the proposed porous obstacle could actually work in transient operation. Issues which could prevent this could be either that the trapping efficiency is too low (so that particles just pass through the obstacle without getting trapped), or that the trapping efficiency is so high that the accumulation of particulates fill up the obstacle before the oxidation reaction can consume the accumulated soot. Ideally, we would like to be able to find a material which traps particles at a rate that is similar to the oxidation rate inside the obstacle.

In the transient filtration model of Konstandopoulos et al. [20], the trapping efficiency over a length Δx in a homogeneous porous material is calculated as:

$$E = 1 - \exp\left(-\frac{3\eta_{DR}(1-\varepsilon)\Delta x}{2\varepsilon d_c}\right). \tag{9.3}$$

Here, η_{DR} is the combined trapping efficiency due to Brownian motion and inertial effects inside the porous material:

$$\eta_{DR} = \eta_D + \eta_R - \eta_D\eta_R, \tag{9.4}$$

where η_D and η_R are determined as

$$\eta_D = 3.5g(\varepsilon)Pe^{-2/3} \tag{9.5}$$

and

$$\eta_R = 1.5N_R^2\frac{[g(\varepsilon)]^3}{(1+N_R)^{(3-2\varepsilon)/3\varepsilon}}, \tag{9.6}$$

respectively. $g(\varepsilon)$ is the geometric function of the unit cell [22]. The local variables ε (porosity) and d_c (the unit collector diameter) are allowed to vary in space and time and are updated according to the expressions given by Konstandopoulos et al. [20].

The oxidation reactions considered are:

$$C + 0.725O_2 \rightarrow 0.45CO_2 + 0.55CO \tag{9.7}$$

and

$$C + 1.5NO_2 \rightarrow 1.5NO + 0.5CO + 0.5CO_2 \tag{9.8}$$

The reaction rates are assumed to be Arrhenius-type functions of temperature, where activation energies and frequency factors are taken from Kandylas and Koltsakis [21]. The enthalpy change due to the chemical reactions is calculated at the current temperature inside each cell in the obstacles and added to the overall heat balance, so that local heat effects are accounted for.

The soot is represented by a diffusing species with a molar mass equal to that of pure carbon. The inlet mass fraction of each species is given in Table 1. The soot mass fraction is chosen so that the inflow of soot into the channel is 50 mg m^{-3}, although this admittedly can be expected to vary much depending on the current engine operating conditions. The total NO_x level is assumed to be 250 ppm and consist entirely of NO_2. This NO_2 would typically come from the engine out NO which is being oxidized over the oxidation catalyst and possibly also catalytic material inside the porous obstacles. Since the conversion of NO to NO_2 has a maximum at 300 °C this assumption is reasonable [21].

Table 1
Inlet mass fraction used in the detailed investigation of the porous obstacles.

Species	Inlet mass fraction
CO	200 ppm
CO_2	5%
NO	–
NO_2	250 ppm
O_2	10%
Soot	82 ppm
N_2	(balance)

Some assumptions on the characteristics of the porous material are also necessary. The initial porosity of the material is assumed 50%. The pore diameter of the porous material is assumed 10 μm. These values are typical of the materials used in wall-flow filters today.

9.6. Irregular channels (Design 5)

The heat and momentum transfer properties of a 'tortuous path' design has been investigated using two-dimensional CFD simulations by Aniolek [23]. Here, we will consider the mass transfer properties of a similar design in three dimensions. A full three-dimensional simulation will reveal also effects of secondary flow, if present. Fig. 11 illustrates the layout of Design 5.

9.7. Fishbone pattern (Design 6)

Design 6 is suggested with inspiration from plate heat exchangers with diagonal flow plates. It is illustrated in Fig. 12.

10. Results and discussion

The six channel designs exemplified above are all of equal length (180 mm). The inlet velocity is 10 m s^{-1} uniformly over the whole cross-section. The outlet pressure is 101,325 Pa and the walls exhibit no slip. The trapping efficiency (E) and channel pressure drop (ΔP) is monitored for each design.

10.1. Design 1

The effects of decreasing the channel diameter are shown in Fig. 13. In effect, almost all 5 nm particles may be trapped by decreasing the hydraulic diameter by approximately one order of magnitude. However, this highly effective mass transfer comes at the expense of a much higher pressure drop.

The theoretical estimations and the CFD simulations agree very well. The former are based on empirical correlations and use only averaged values from the monolith channel. In the CFD simula-

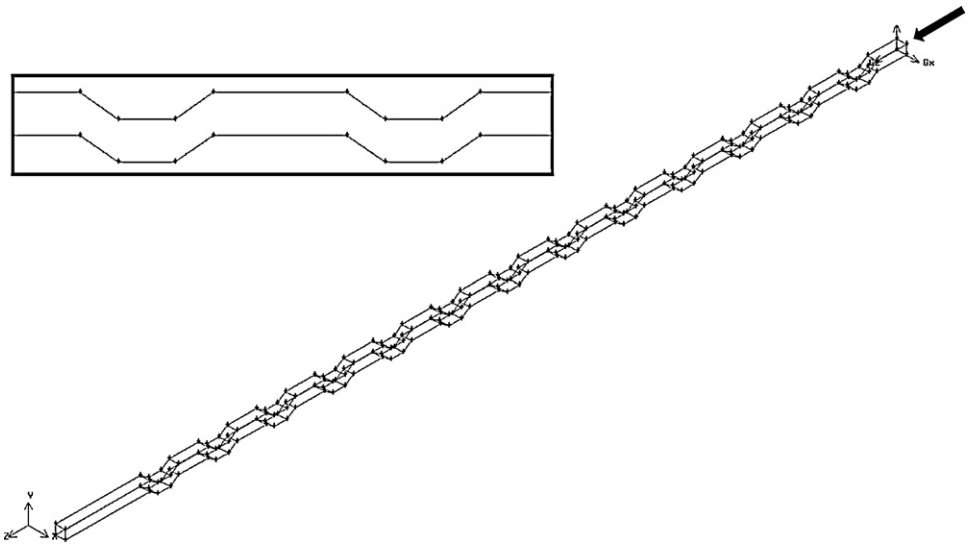

Fig. 11. The layout of Design 5. The exhaust enters through the inlet at the upper right and flows through the tortuous channel and exits at the outlet in the lower left. The length of the channel is 180 mm and each side in the cross-section is 2 mm. The boxed figure shows the tortuous pattern in greater detail. The black arrow indicates the inlet gas flow direction.

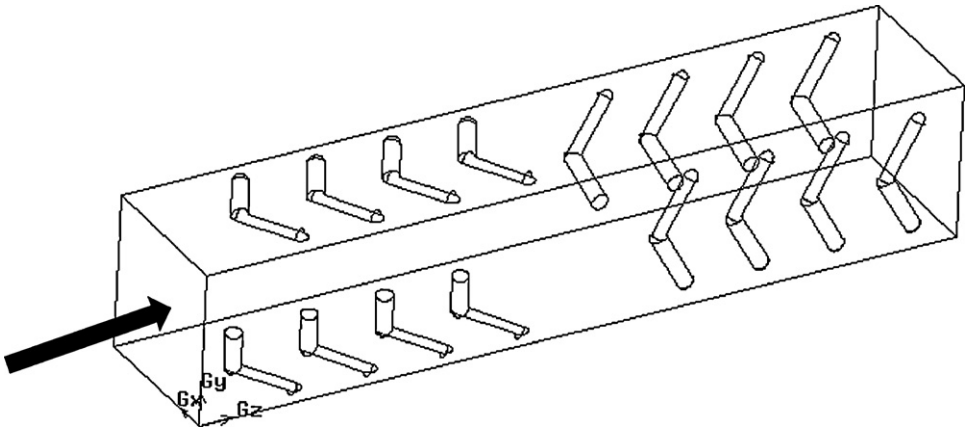

Fig. 12. The layout of Design 6. The entire channel consists of 18 segments such as the one shown here. Each diagonal pattern is 0.1 mm deep and the hydraulic diameter of the channel is 2 mm. The black arrow indicates the inlet gas flow direction.

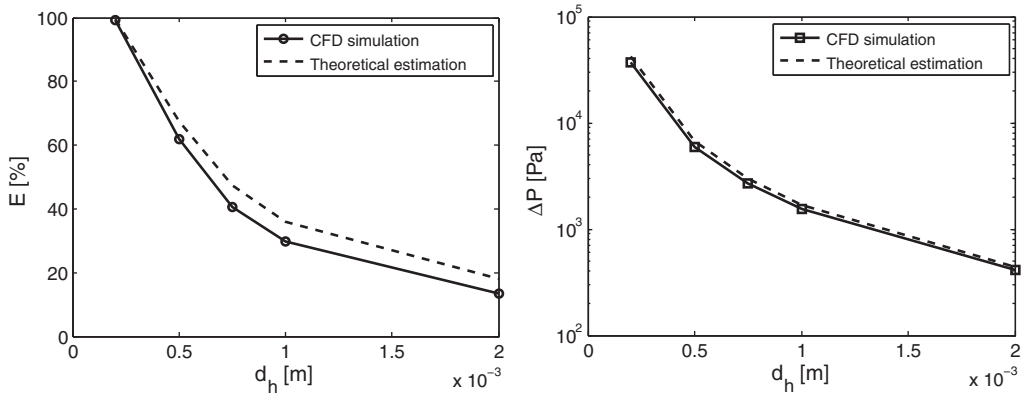

Fig. 13. The particle trapping efficiency (E; to the left) and the pressure drop (ΔP; to the right) as a function of the hydraulic diameter for straight monolith channels with square cross-section (Design 1). Both the results of the CFD simulations and the theoretical estimations described in Section 9.2 are shown.

tions, the entire pressure and velocity fields are available directly. Also the development of the laminar flow profile is inherently taken into account in the CFD simulations. In summary, these results supports the strength of using CFD to obtain results for channel designs where experimental data is not available.

10.2. Design 2

The trapping efficiency for 5 nm particles in the design with parallel plates is 68%. The corresponding pressure drop is 4560 Pa. When compared to Design 1, it is evident that Design 2 provides

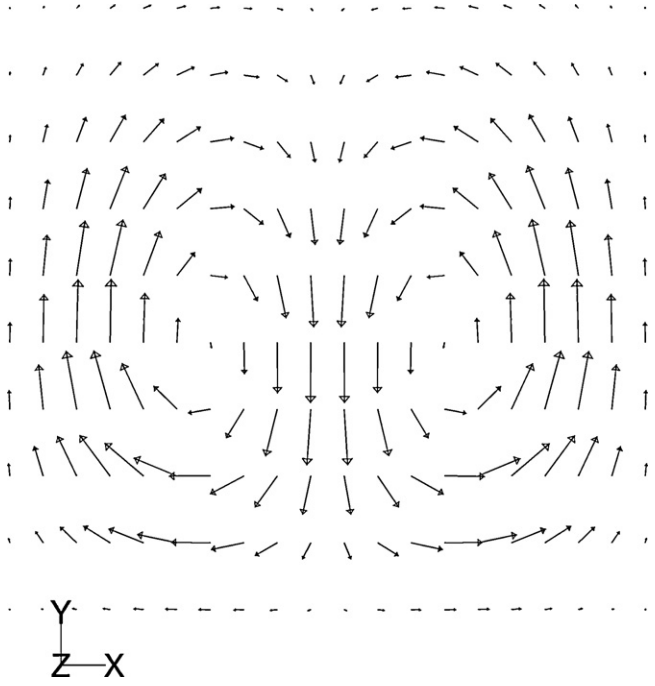

Fig. 14. Velocity vectors in a plane perpendicular to the main flow direction after the first obstacle in Design 3. The plane is placed approximately 25 mm after the preceding obstacle.

a means to achieving a lower effective distance for transport but without imposing the same penalty on the pressure drop. With the plates inside, the 2 mm diameter channel shows a trapping efficiency corresponding to approximately an effective diameter of 0.45 mm (cf. Fig. 13). This would correspond to a pressure drop of approximately 8100 Pa in a design with straight channels, which means that the pressure drop in Design 2 is about 44% lower for the same trapping efficiency.

10.3. Design 3

The existence of flow loops is confirmed from the solution of the fluid flow in the Design 3 channel. An illustration of the flow loop after the first obstacle is provided in Fig. 14 for comparison with Fig. 8. The particle trapping efficiency for 5 nm particles is 21% and the pressure drop over the channel length is 526 Pa.

10.4. Design 4

The pressure drop and the particle trapping efficiency when the obstacles in Design 3 are treated as porous media, are plotted in Fig. 15 for different values of the permeability. There is a very clear change taking place between permeabilities of order of magnitude from 10^{-10} to 10^{-8}. For very low permeabilities, the obstacles are virtually impermeable to the gas flow. The trapping efficiency is then the same as for solid obstacles. For high permeabilities, the gas can flow more easily through the obstacles, and the trapping efficiency goes up. However, the assumption that all particles entering a porous obstacles will get trapped becomes more improbable with increasing permeability. There is thus a threshold value of the permeability above which the assumptions underlying the results presented in Fig. 15 are most probably violated. Therefore, a more detailed investigation was also carried out using the models of Konstandopoulos et al. [20] and Kandylas and Koltsakis [21].

The case that is chosen for this more detailed investigation is the one with a permeability of 10^{-9} m^2. The screening model predicts a significant increase in particle trapping for this choice compared to when the obstacles are solid. For 5 nm particles, the trapping efficiency increases from 21% to 46%, an increase of approximately 120%.

The outlet mass fraction of soot is therefore also predicted using the submodels of Konstandopoulos et al. [20] and Kandylas and Koltsakis [21]. Three temperatures (200, 300 and 400 °C) were evaluated. It turns out that the oxidation reaction with NO_2 quickly consumes the trapped particles inside the obstacles already at the lowest temperature. That is, the depletion of collected particles is much faster than the rate at which particles are accumulated in the obstacles. Although further investigation of the performance of this design for wider temperature and inlet soot mass fraction ranges must be undertaken, these results illustrate the potential of computational screening of different designs. Given additional experimental confirmation, the final channel design may be found by an optimization procedure using the herein suggested models.

10.5. Design 5

The trapping efficiency of 5 nm particles in Design 5 is 41%. The pressure drop over the entire channel is then approximately 1010 Pa. When compared to Design 1, the trapping performance is equivalent to a straight channel of 0.74 mm diameter. The pressure drop is however 65% lower.

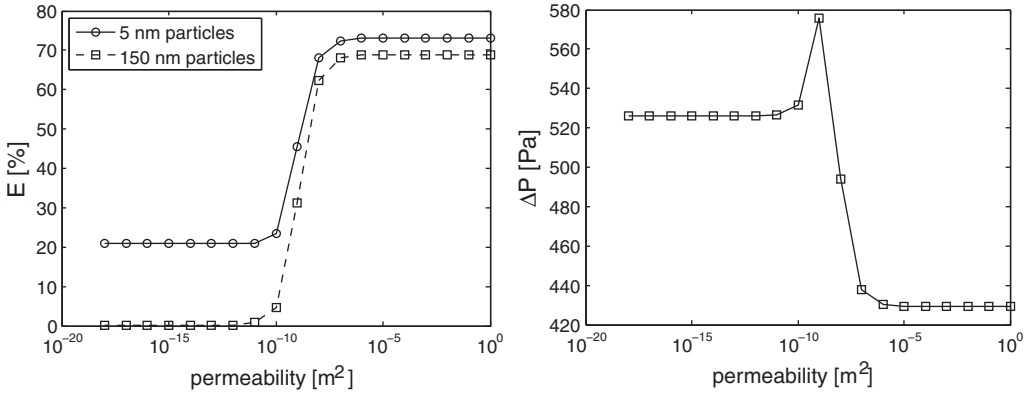

Fig. 15. The particle trapping efficiency (E; to the left) of 5 nm and 150 nm particles and the pressure drop (ΔP; to the right) as a function of the permeability of the porous obstacles (Design 4).

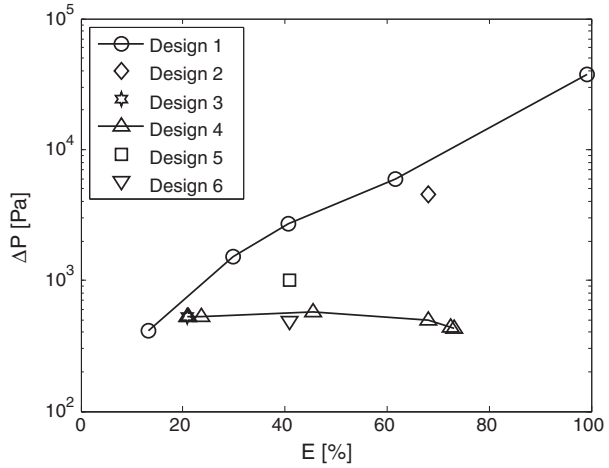

Fig. 16. A summary of the results for Designs 1–6. The pressure drop is plotted against the particle trapping efficiency of 5 nm particles as predicted by the screening model. For Design 1, the line connects the results of the different channel diameters. For Design 4, the line connects the results of the different obstacle permeabilities.

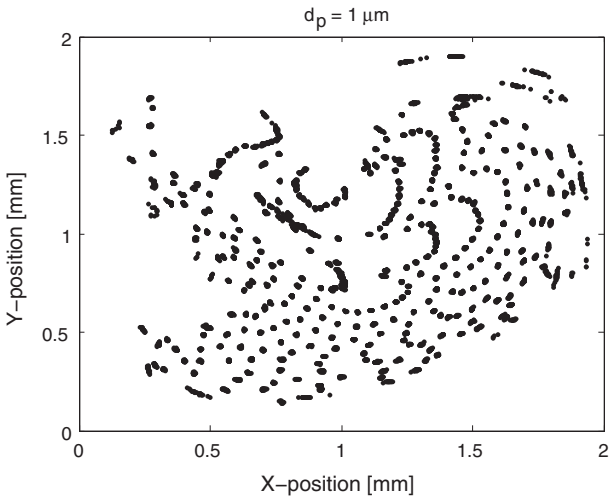

Fig. 17. Illustration of inertial effects in Design 3 for particles of size 1 μm: particle distribution at the channel outlet. (The size of the plotted particles is greatly exaggerated compared to their real size.)

10.6. Design 6

The trapping efficiency of 5 nm particles in Design 6 is 41%. The pressure drop over the entire channel is then approximately only 489 Pa. This design is thus much better than Design 5, which has the same trapping efficiency but more than twice the pressure drop.

10.7. Results map

The results can be summarized in a results map, where the imposed pressure drop is plotted against the obtained trapping efficiency. The best designs will then appear in the lower right of the diagram. The results map for Designs 1–6 is shown in Fig. 16.

A conventional wall-flow filter would appear in the upper right of the diagram (high trapping efficiency and high pressure drop). The pressure drop is very dependent on the current soot content in the filter, but is typically in the interval 10^4 to 3×10^5 [19], for which over 95% trapping efficiency may be obtained.

Most of the designs investigated in the current work are similar to designs already available commercially today, or exploit design features (e.g. porous materials, ultra-thin walls) that have previously been used in commercial catalysts (albeit differently) [23–26]. As for the novelties suggested here, we therefore believe that they are within reach of what is currently manufacturable.

10.8. Inertial effects

The designs were also investigated using the full model of Ström and Andersson [5] in order to reveal where significant inertial effects were present. Particles of a size of one micrometer were used for this purpose. It was found that only in very few circumstances did these particles possess enough inertia to deviate noticeably from the fluid streamlines. One such circumstance was however in the designs with obstacles. Even though there is no significant effect on the overall particle trapping efficiency, the patterns of the positions of individual particles revealed by the elaborate model clearly proves the influence of inertia.

As an illustration, we plot the distribution of particles on the outlet of the channel with solid obstacles. As can be seen from Fig. 17, the large particles possess enough inertia to have formed clusters depending on the exact motion of the fluid streamlines. The screening model cannot capture the inertial effects and thus predicts an even distribution of particles over the outlet.

Judging from the clusters of particles in Fig. 17, the flow loops created by the introduction of obstacles as in Design 3 could potentially be further optimized to increase the trapping of larger particles in such a design by properly utilizing this effect.

Whereas it was initially speculated that Design 5 would exhibit increased trapping efficiency of larger particles due to the 'tortuous path', this was proven wrong when investigated. There was in fact no significant trapping of larger particles in that design at all.

11. Summary and conclusions

Two radically different models for estimation of the particle trapping efficiency in an automotive catalyst have been evaluated. The two models are combined into a third, hybrid model which allows for accurate and computationally efficient predictions of the particle trapping performance of an automotive catalyst design.

For fast scanning of different designs, the simplified screening model proposed in this work is recommended. It is shown to accurately reproduce the trapping efficiencies for small (<50 nm) particles when compared to the more detailed model.

A number of alternatives to the standard monolith channel design have been suggested and evaluated using the screening model. It is shown that there is great potential in several of them to increase the particle trapping efficiency without radically increasing the pressure drop over the monolith. The optimization of any of the herein suggested designs could preferably be carried out with the simplified screening model. The suggested procedure can be used to single out promising candidates for automotive catalyst design whilst dramatically reducing the time necessary from idea to pilot scale testing. In particular, a design with porous obstacles of a material whose permeability to fluid flow is on the order of 10^{-9} m^2 showed promising results. Provided that adequate experimental validation can now be obtained, the herein presented method provides new possibilities for simulation-driven design of automotive catalysts with soot trapping capabilities.

The current work thus contains both an in-depth study of the phenomena that governs the performance of these devices, as well as computationally efficient tools to optimize the devices themselves.

Acknowledgements

This work has been performed within the Competence Centre for Catalysis, which is financially supported by Chalmers University of Technology, the Swedish Energy Agency and the member companies: AB Volvo, Volvo Car Corporation, Scania CV AB, GM Powertrain Sweden AB, Haldor Topsoe A/S and The Swedish Space Corporation. Rodrik Fällmar is greatfully acknowledged for his master thesis, *Design of an optimal oxidation catalyst for particle trapping*, in which many of the ideas presented here were first tested.

References

[1] WHO Working Group, Health Aspects of Air Pollution with Particulate Matter, Ozone and Nitrogen Dioxide. Report on a WHO Working Group, Bonn, Germany, 13–15 January, 2003.
[2] European Parliament, Regulation (EC) No 715/2007 of the European Parliament and of the Council of 20 June 2007 on type approval of motor vehicles with respect to emissions from light passenger and commercial vehicles (Euro 5 and Euro 6) and on access to vehicle repair and maintenance information. OJ L 171, 29.6.2007, 1.
[3] J.-H. Lee, Y. Goto, M. Odaka, Measurement of the Diesel Exhaust Particle Reduction Effect and Particle Size Distribution in a Transient Cycle Mode with an Installed Diesel Particulate Filter (DPF). SAE Technical Paper 01-1005, 2002.
[4] J. Yang, M. Stewart, G. Maupin, D. Herling, A. Zelenyuk, Single wall diesel particulate filter (DPF) filtration efficiency studies using laboratory generated particles, Chem. Eng. Sci. 64 (2009) 1625–1634.
[5] H. Ström, B. Andersson, Simulations of trapping of diesel and gasoline particulate matter in flow-through devices, Top. Catal. 52 (2009) 13–20.
[6] K. Ohno, K. Shimato, N. Taoka, H. Santae, T. Ninomiya, T. Komori, O. Salvat, Characterization of SiC-DPF for Passenger Car. SAE Technical Paper 01-0185, 2000.
[7] D.B. Kittelson, Engines and nanoparticles: a review, J. Aerosol Sci. 29 (1998) 575–588.
[8] H.L. Langhaar, Steady flow in the transition length of a straight tube, Trans. Am. Soc. Mech. Eng. 64A (1942) 55–58.
[9] S. Chandrasekhar, Stochastic problems in physics and astronomy, Rev. Modern Phys. 15 (1943) 1–89.
[10] A. Einstein, On the motion of small particles suspended in liquids at rest required by the molecular-kinetic theory of heat, Ann. Phys. 17 (1905) 549–560.
[11] J.E. Johnson, D.B. Kittelson, Deposition, diffusion and adsorption in the diesel oxidation catalyst, Appl. Catal. B 10 (1996) 117–137.
[12] C. Crowe, M. Sommerfeld, Y. Tsuji, Multiphase Flows with Droplets and Particles, CRC Press, 1998.
[13] S.L. Andersson, N.-H. Schöön, Methods to increase the efficiency of a metallic monolithic catalyst, Ind. Eng. Chem. Res. 32 (1993) 1081–1086.
[14] R.D. Hawthorn, Afterburner catalysts – effects of heat and mass transfer between gas and catalyst surface, AIChE Symp. Ser. 137 (1974) 428.
[15] Ekström, Andersson, Pressure Drop of Monolithic Catalytic Converters. Experiments and Modeling. SAE Technical Paper 01-1010, 2002.
[16] Cutler, Merkel, A New High Temperature Ceramic Material for Diesel Particulate Filter Applications. SAE Technical Paper 01-2844, 2000.
[17] Y. Choi, Z. Dang, R. Stone, M. Morrill, D. Floyd, New Flow-Through Trap System Targeting 50% PM Removal for Diesel Emission Control. SAE Technical Paper 01-0232, 2007.
[18] Purem GmbH, Sintered Metal Filter For Commercial Vehicle Exhaust Aftertreatment, Purem GmbH, Menden, Germany, 2002.
[19] A. Suresh, A. Khan, J.H. Johnson, An Experimental and Modeling Study of Cordierite Traps – Pressure Drop and Permeability of Clean and Particulate Loaded Traps. SAE Technical Paper 01-0476, 2000.
[20] A.G. Konstandopoulos, M. Kostoglou, E. Skaperdas, E. Papaioannou, D. Zarvalis, E. Kladopoulou. Fundamental Studies of Diesel Particulate Filters: Transient Loading, Regeneration and Aging. SAE Technical Paper 01-1016, 2000.
[21] I.P. Kandylas, G.C. Koltsakis, NO_2-assisted regeneration of diesel particulate filters: a modeling study, Ind. Eng. Chem. Res. 41 (2002) 2115–2123.
[22] K.W. Lee, J.A. Gieseke, Collection of aerosol particles by packed beds, Environ. Sci. Technol. 13 (1978) 1761.
[23] K.W. Aniolek, A CFD Study of Diesel Substrate Channels with Differing Wall Geometries. SAE Technical Paper 01-0152, 2004.
[24] P. Flörchinger, M.G. Ortiz, R. Ingram-Ogunwumi, Comparative Analysis of Different Heavy Duty Diesel Oxidation Catalysts Configurations. SAE Technical Paper 01-1419, 2004.
[25] A.K. Jindal, N. Bhate, A. Shukla, R. Jain, B. Ghosh, C.F. Dias, S.A. Waje, H.D. Rasal, A. Reck, P. Treiber, Application of Continuously Regenerating Metallic PM Filter Catalyst on Commercial Vehicles with Direct Injection Diesel Engines. SAE Technical Paper 26-022, 2005.
[26] L. Pace, M. Presti, Changing the Substrate Technology to meet Future Emission Limits. SAE Technical Paper 01-1550, 2004.